*Proc. Natl. Acad. Sci. USA*
Vol. 96, pp. 3670–3675, March 1999
Biophysics

# Single-pair fluorescence resonance energy transfer on freely diffusing molecules: Observation of Förster distance dependence and subpopulations

ASHOK A. DENIZ*†, MAXIME DAHAN†‡, JOCELYN R. GRUNWELL*, TAEKJIP HA‡§, ANN E. FAULHABER*, DANIEL S. CHEMLA‡¶, SHIMON WEISS‡‖**, AND PETER G. SCHULTZ*,**

*Howard Hughes Medical Institute, Department of Chemistry, and ¶Department of Physics, University of California, Berkeley, CA 94720; and ‡Materials Sciences Division, and ‖Physical Biosciences Division, Lawrence Berkeley National Laboratory, Berkeley, CA 94720

*Contributed by Daniel S. Chemla, January 21, 1999*

**ABSTRACT** **Photon bursts from single diffusing donor-acceptor labeled macromolecules were used to measure intramolecular distances and identify subpopulations of freely diffusing macromolecules in a heterogeneous ensemble. By using DNA as a rigid spacer, a series of constructs with varying intramolecular donor-acceptor spacings were used to measure the mean and distribution width of fluorescence resonance energy transfer (FRET) efficiencies as a function of distance. The mean single-pair FRET efficiencies qualitatively follow the distance dependence predicted by Förster theory. Possible contributions to the widths of the FRET efficiency distributions are discussed, and potential applications in the study of biopolymer conformational dynamics are suggested. The ability to measure intramolecular (and intermolecular) distances for single molecules implies the ability to distinguish and monitor subpopulations of molecules in a mixture with different distances or conformational states. This is demonstrated by monitoring substrate and product subpopulations before and after a restriction endonuclease cleavage reaction. Distance measurements at single-molecule resolution also should facilitate the study of complex reactions such as biopolymer folding. To this end, the denaturation of a DNA hairpin was examined by using single-pair FRET.**

During the past decade, spectacular progress has been made in the field of single-molecule fluorescence detection (1–3). Single-molecule experiments enable us to study physical, chemical, or biological properties of molecules on a truly molecular basis, in contrast to conventional methods, which only provide ensemble averaged data. Thus, single-molecule experiments allow a direct comparison to theory, which usually analyzes systems at the microscopic level.

Single fluorescently tagged biomolecules can be detected when they are freely diffusing or flowing in solutions or when they are immobilized (surface attached or imbedded in matrices or droplets), providing different and complementary kinds of information. With immobilized molecules, the evolution of a property for a particular molecule over an extended period of time can be studied. This allows, for example, the observation of its dynamic fluctuations under equilibrium conditions, or acquisition of its full time-trajectory during a reaction (4). However, care must be taken to ensure minimal perturbation from the immobilization.

When diffusing or flowing single molecules in a liquid traverse the laser excitation volume, fluorescence photon bursts are generated. Such bursts can be analyzed for their brightness, duration, spectrum, and fluorescence lifetime, thereby providing molecular information on identity, size, diffusion coefficient, and concentration (5–7). These bursts are short (millisecond) and provide less information on slower conformational dynamics. However, they can provide invaluable information about the distributions of molecular properties of interest, undisturbed by surface effects. Because a large number of events (photon bursts) can be collected in a relatively short time, statistical analysis of these data is possible and histograms can be constructed. Most importantly, subpopulations of analyte molecules in heterogeneous ensembles can be identified and separated (8, 9).

A closely related technique, fluorescence correlation spectroscopy, also has been used to analyze, sort, and detect conformational states of a few or single molecules in the excitation volume (7, 10–13). However, because it relies on the autocorrelation function, a considerable amount of temporal information is disregarded.

So far, most single-molecule burst studies have been limited to measuring distributions in burst size or in fluorescence lifetime. Two-color burst analysis (14, 15), two-color fluorescence correlation spectroscopy (15), and multiple-lifetime (8) approaches for identification and separation recently have been suggested and implemented, but no attempts to separate subpopulations by ratiometric methods have been made. In the work described here, a ratiometric observable, single-pair fluorescence resonance energy transfer (spFRET) (16), is measured to obtain distributions in energy transfer efficiency of freely diffusing single molecules. Ratiometric measurements are particularly useful in such systems because the effects of intensity fluctuations, inherent to the single-molecule regime, are minimized. Besides FRET, other molecular properties can be interrogated by using such a two-channel detection scheme, and subpopulations can be efficiently distinguished.

## MATERIALS AND METHODS

**Sample Preparation.** *DNA synthesis.* For the distance dependence study, dyes were conjugated to a 40-bp-long random sequence, as shown in Fig. 1*a Inset*. Oligonucleotide 1, the upper one shown there, has the sequence 5′-CTCTTCAGTTCACAGTCCATCCTATCAGCCGCTTGCCTTC-3′; oligonucleotide 2 is its complement. Reagents for oligonucleotide synthesis are from Glen Research, Sterling, VA. In the DNA 16 construct, tetramethylrhodamine (TMR) *N*-hydroxysuccinimide (NHS) ester was conjugated to a 3′ amino modifier on oligonucleotide 2 and Cy5 NHS ester to an amino modifier C6

The publication costs of this article were defrayed in part by page charge payment. This article must therefore be hereby marked "*advertisement*" in accordance with 18 U.S.C. §1734 solely to indicate this fact.

PNAS is available online at www.pnas.org.

Abbreviations: FRET, fluorescence resonance energy transfer; spFRET, single-pair FRET; TMR, tetramethylrhodamine.

†A.A.D. and M.D. contributed equally to this work.

§Present address: Department of Physics, Stanford University, Stanford, CA 94305.

**To whom reprint requests should be addressed. e-mail: pschultz@lbl.gov or sweiss@lbl.gov.

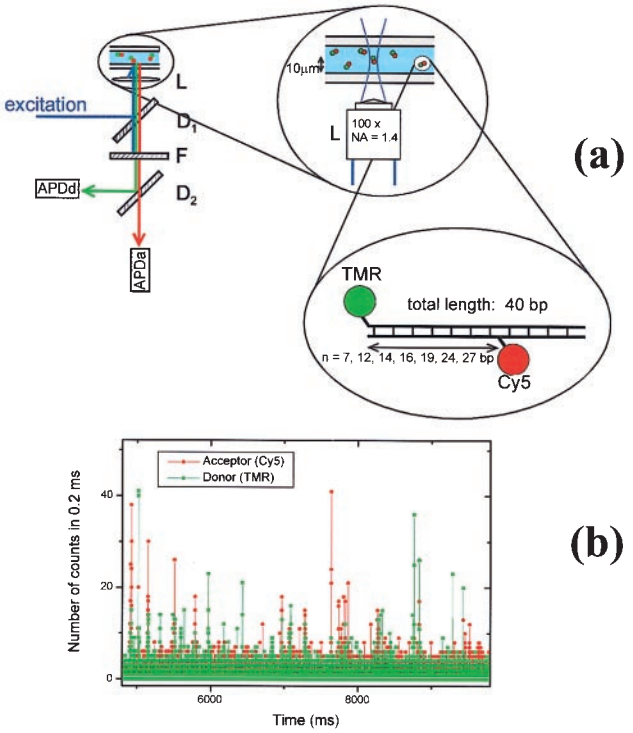


FIG. 1. (*a*) Experimental setup for diffusion spFRET. L is the objective, $D_1$ and $D_2$ are dichroic mirrors centered at 530 and 630 nm, respectively, and F is a notch filter. (*Inset*) The DNA *n* constructs used for the FRET distance study. TMR is attached to one end of the DNA and CY5 is attached to the *n*th base from the end. (*b*) Dual (donor and acceptor) channel time traces for DNA 12 freely diffusing in solution. Fluorescence bursts above background are clearly visible as molecules traverse the laser beam. The conditions used were 30 pM DNA concentration, 0.6 mW, 514 nm laser light focused 10 $\mu$m into the solution from the coverslip surface and a 0.2-ms integration time.

dT at position 16 of oligonucleotide 1. For the other DNA constructs, TMR maleimide was conjugated to a 5′ thiol modifier C6 on oligonucleotide 1, and Cy5 was covalently attached to an amino modifier C6 dT at the appropriate position (nos. 7, 12, 14, 19, 24, or 27) of oligonucleotide 2. The oligonucleotides were synthesized by using standard phosphoramidite chemistry and purified by using C18 reverse-phase HPLC. The sequence of the hairpin is 5′-ATC-CTATTTTTTTAGGAT-3′. A 5′ thiol for TMR attachment and an amino modifier C6 dT for Cy5 attachment at position 13 were incorporated as described above.

*TMR–maleimide labeling of the 5′ thiols.* The silver nitrate deprotected thiol was purified and reacted with TMR–maleimide for 2 hr (in sodium phosphate buffer, 100 mM NaCl, pH 7.2). The labeled oligonucleotide was purified by using a NAP-5 column followed by reverse-phase HPLC. Size-exclusion FPLC was used in some cases to separate out residual free dye from the labeled oligonucleotide.

*TMR/Cy5–*N*-hydroxysuccinimide* (*NHS*) *ester labeling of amines*. The amine modified oligonucleotide was reacted with the NHS ester for 2–8 hr (in 100 mM sodium bicarbonate buffer, pH 9) and purified as for the TMR maleimide labeling reaction.

*Double-stranded DNA.* For FRET experiments, double-stranded DNA was made by mixing together TMR and Cy5 labeled complementary strands in a 1:1.5 ratio in 20 mM sodium phosphate, 1 M NaCl, pH 7, heating to 95°C and cooling to 4°C over 30 min. It is estimated that these double-stranded DNA samples contain less than 5–10% of free TMR or TMR-labeled single strand. Double-stranded DNA singly labeled with TMR or Cy5 was made in a similar fashion.

*Restriction enzyme digests.* The DNA sequence used is 5′-GCAGTGGAATTCGCGATGGTTAGGATGTGTGAAC-TGAATG-3′ with an amino modifier C6 dT at position 17 for Cy5 attachment. The complementary strand has a 3′ amino modifier for TMR attachment. DNA was incubated at 37°C for 3–5 hr with 20 units of *Eco*RI enzyme (NEB, Beverly, MA) in *Eco*RI buffer.

**Confocal Microscope Setup.** The apparatus used for the single-molecule detection experiments has been described in detail (18). Briefly, it consists of an inverted confocal microscope (Zeiss Axiovert SV 100) coupled to a high-sensitivity detection setup as shown in Fig. 1*a*. A small volume (10 $\mu$l) of sample solution is placed between two glass coverslips and laser light (514 nm line of an Argon ion laser) is focused on it by using a high numerical aperture objective (L, Zeiss 100×, NA 1.4, oil immersion). To detect freely diffusing molecules, the focal point is placed within the sample solution, about 10 $\mu$m from the glass coverslip surface. The fluorescence light is collected through the same objective and imaged onto a pinhole to reject out-of-focus light. The fluorescence then is split by a dichroic mirror into two parts, which are separately focused onto two avalanche photodiodes (*APDa* and *APDd*, EG&G, Vaudreuil, SPCM AQ-141), coupled to a counting board and a personal computer. The overall detection efficiency in water and 10 $\mu$m away from the interface is estimated to be around 1%. The FRET pair is composed of TMR (donor, peak emission at 575 nm) and Cy5 (acceptor, peak emission at 670 nm), whose fluorescence is separated by using a dichroic mirror centered at 630 nm ($D_2$, Omega Optical, Brattleboro, VT, DRLP630). The large extinction coefficient of Cy5 (250,000) allows a good spectral separation while maintaining a large $R_0$ of about 53 Å. To ensure the single-molecule regime, a typical concentration of molecules in the sample of 30 pM is used. Under these conditions, in a diffraction-limited excitation volume of about 0.5 fl, the single-molecule occupancy probability is about 0.01 and is much larger than the probability of simultaneously having two molecules ($5 \times 10^{-5}$).

**Inter-Dye Distances–Helical Model of DNA.** In a simple cylindrical description of the B form DNA double helix (see Fig. 2*b, Inset*), the typical diameter is 20 Å, the rise per bp is 3.4 Å, and 10 bp make a turn (21). The inter-dye distance, $R$, is calculated as a vector sum of components parallel ($R_a$) and perpendicular ($R_b$) to the cylinder axis (19, 20), which is illustrated in Fig. 2*b, Inset*. $R_a$ ($= 3.4\,N + L$) is a function of the bp separation $n$ ($N = n - 1$), and $L$, the distance between the dyes for $n = 1$. $R_b$ [$= a^2 + d^2 + 2ad\cos(\theta)$] is a function of $a$ and $d$, the acceptor and donor distances from the axis and the angular separation $\theta$ ($= 36\,N + \phi$), as shown. $\phi$ is the inter-dye angular separation for $n = 1$. Note that this model does not account for sequence-dependent variation in the structure or fluctuations in the distance caused by fluctuations in the tethers, DNA, or breathing and transient partial melting of the DNA. Given the resolution in our FRET efficiency data, our results are not sensitive enough to measure such deviations. Furthermore, we do not attempt to fit the data with the four-parameter model presented here, but instead use reasonable estimates based on the structural properties of the dyes and their tethers ($a = d = 15$ Å, $L = 5$ Å and $\phi = 225°$).

## RESULTS AND DISCUSSION

**spFRET.** For the last three decades, FRET has been extensively used to make distance measurements in biological systems. FRET is the nonradiative transfer of electronic excitation energy from donor to acceptor dye molecules by a weak dipole-dipole coupling mechanism. The transfer efficiency was predicted by Förster to decrease with $R$, the distance between the two dyes, as $1/(1+(R/R_0)^6)$ (22). $R_0$, the Förster radius, is the distance corresponding to 50% energy transfer and depends on the photophysical properties of the

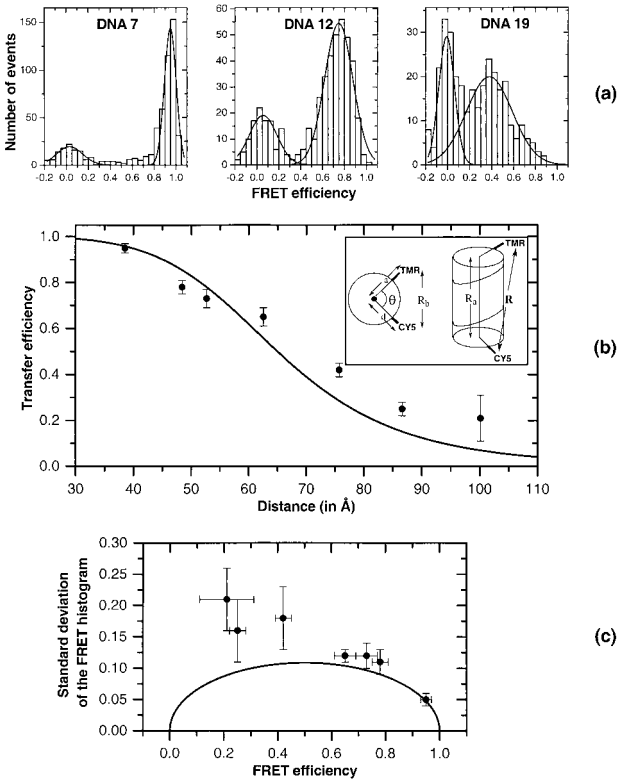


FIG. 2. (*a*) FRET histograms extracted from time traces for DNAs 7, 12, and 19 using a threshold of 20. Double gaussian fits extract numbers for the mean (width) of the higher efficiency peak of 0.95 (0.05), 0.75 (0.13), and 0.38 (0.21) respectively. (*b*) Mean FRET efficiencies extracted from FRET histograms plotted as a function of distance for the seven DNA constructs, DNAs 7, 12, 14, 16, 19, 24, and 27. Distances are calculated by using the model shown in the *Inset* and discussed in *Materials and Methods*. The error bars represent two SDs ($\pm 1\sigma$) from multiple measurements and increase with distance. The solid line is the theoretical curve with $R_0 = 65$ Å for comparison. (*c*) Mean widths extracted from the histograms are plotted as a function of the mean FRET efficiencies. The *x*-axis error bars are the same as in *b*. The *y*-axis error bars represent two SDs ($\pm 1\sigma$) from multiple measurements. The solid line shows widths calculated by using a simple model for the effect of shot noise, as described in the text.

dyes and their relative orientations. Ever since Stryer and Haughland (23) demonstrated this distance dependence, FRET has been used as a spectroscopic ruler in ensemble experiments. It allows distance measurements on the 20- to 80-Å scale and hence is well suited to study conformations of biological macromolecules. At the single-molecule level, FRET recently has been observed between two dyes on a dry surface (16) and has been applied to ligand-receptor colocalization on a membrane (24) and to study immobilized proteins and protein-DNA interactions in solution (25).

spFRET measurements can be used to probe not only average distances as in an ensemble experiment, but also to directly observe distributions and the time evolution of conformational (distance) properties. Though dynamics can be followed in ensemble experiments on systems with simple behavior, it is impossible to maintain the synchronization necessary for such experiments in more complex or stochastic systems. Processes such as protein folding, biopolymer fluctuations, and enzyme kinetics can be fully characterized only at the single-molecule level; hence, it is essential to develop single-molecule FRET methodologies to an extent that will allow such measurements. The ability to identify subpopulations also will prove useful in analytical chemistry applications (26). At a more fundamental level, single-molecule FRET experiments also can provide information about the energy transfer process itself (such as detailed photon arrival statistics and correlations between the donor and the acceptor states, correlated quantum jumps) that will directly probe the quantum nature of the donor-acceptor system.

Previous spFRET studies of immobilized molecules (16, 25) demonstrated the potential of the technique for the study of dynamic distance changes. However, they also showed that spFRET under those conditions performs poorly with respect to static distance measurements because of dye and macromolecule interactions with the surface. Hence, no systematic distance dependence of spFRET was observed. Toward this end, a methodology that extends spFRET to observations on freely diffusing single molecules, free from perturbations introduced by surface interactions, was developed and is presented here. The distance dependence of Förster energy transfer (FRET) is demonstrated on the single-molecule level, subpopulations in a mixture of molecules with different donor-acceptor distances are identified, changes in substrate-product subpopulations caused by an enzymatic reaction are followed, and the unfolding reaction by urea denaturation of a DNA hairpin is measured. The resolving power and the limitations of the technique also are discussed.

**Distance Dependence.** The persistence length of duplex B-form DNA is about 500 Å (27), allowing it to be used as a rigid spacer for donor-acceptor attachment at distances relevant to FRET experiments (20–80 Å). A set of test systems with varying donor-acceptor bp separations was synthesized to investigate the distance dependence on the single-molecule level. To compare the measured FRET efficiencies with Förster theory, this bp separation was converted into distances by using the model introduced for DNA-FRET analysis by Clegg and coworkers (19). Given the estimated Förster radius of 53 Å for the TMR-Cy5 dye pair, seven doubly labeled DNA constructs were examined with 7-, 12-, 14-, 16-, 19-, 24-, and 27-bp separations corresponding to distances from 35 Å to 100 Å. These constructs allowed us to study transfer efficiencies ranging from above 90% to about 20%. To keep parameters such as diffusion and melting rates constant over the series, the different DNA constructs had a constant total length of 40 bp. While TMR is at the same end of all of the DNA molecules, Cy5 was attached at different positions within the construct, as shown in Fig. 1*a*. In the rest of the paper, a particular DNA construct is referred to as DNA *n* (for example, DNA 7), where *n* indicates the bp separation between the dyes.

In the experiments, the donor (TMR) was excited, and the donor and acceptor (Cy5) emissions were separately and simultaneously detected. Pairs of data points corresponding to the number of detected photons in the two channels, $I_d$ and $I_a$, were recorded with an integration time of 0.2 ms. Fig. 1*b* shows a time trace of dual detector data for donor-acceptor-labeled DNA 12 molecules. Because of the low concentration, most of the points consist of background signal, resulting predominantly from Raman and Rayleigh scattering and showing a Poisson distribution with a typical mean value below 1 count. The occasional peaks, clearly visible above background in Fig. 1*b*, correspond to single donor-acceptor-labeled DNA molecules diffusing through the focal volume and emitting bursts of photons. The duration of these bursts, on the order of 1 ms, is determined by their diffusion rate, whereas their amplitudes depend on several factors, such as the position of the molecule in the laser spot and the photophysical properties of the dyes. Measurement conditions were carefully optimized by using an autocorrelation criterion presented by Mathies and coworkers (28). Optimal results were obtained by using a 100-$\mu$m pinhole and 0.6-mW laser power and focusing 10 $\mu$m away from the coverslip surface into the liquid sample. Under these conditions, the typical number of collected photons for the most intense signals is around 100 counts per burst.

The time trace shows fluorescence bursts on both the donor and acceptor channels. Because direct excitation of the accep-

tor and leakage of the donor emission into the acceptor channel is small, bursts on the acceptor channel result from Cy5 emission caused by energy transfer. A simple approach is used to extract FRET information from these photon bursts. First, a threshold is used to discriminate dye signal from the background noise, i.e., pairs of data points from time bins $i$ are accepted only when the sum of signals from both channels ($I_a^i + I_d^i$) is above a given theshold $T$. In practice, the threshold value is chosen to effectively reject background while retaining as many points as possible. Above a certain value (on the order of 20 counts for 0.2-ms integration time), changes in the threshold result in changes in the total number of events but not in the mean peak position. For the accepted events, the FRET efficiencies, $E^i = I_a^i/(I_a^i + \gamma I_d^i)$, are computed and collected in a histogram (Fig. 2*a*). The factor $\gamma$ is equal to $\eta_a\phi_a/\eta_d\phi_d$ and accounts for the effects of donor and acceptor quantum yields ($\phi_a$ and $\phi_d$) as well as their respective collection efficiencies ($\eta_d$ and $\eta_a$). This factor, although difficult to measure, has been estimated to be about 1 for surface immobilized TMR-Cy5 (25), the value used in this paper.

Fig. 2*a* shows three representative FRET efficiency histograms that were generated from photon-burst data for DNAs 7, 12, and 19. A noticeable feature in each of these histograms is the presence of two peaks, one centered at around zero efficiency and a second at higher efficiency. By using an oxygen scavenging system (29), the zero efficiency peak was reduced by a factor of about 4, suggesting its origin in accelerated photobleaching of acceptors leaving behind donor-only labeled molecules. The remaining fractions of the zero peak probably come from residual photobleaching, nonideal purification, and possibly nonfluorescent Cy5 species. Acceptor triplet states also might contribute to the zero peak. The second peak clearly shifts to lower FRET efficiency with increasing inter-dye distance (bp separation), as expected for Förster energy transfer.

To extract the mean value and width of the FRET efficiencies, the contribution of the second (higher efficiency) peak was separated out by carrying out a double gaussian fit to the histograms.†† The numbers extracted from the histograms are given in Fig. 2*a*. Because the widths of these distributions are about 0.1–0.2 $E$ (energy transfer) units, it is hard to separate out FRET peaks with means smaller than $\approx$0.4 $E$ because of considerable overlap with the photobleaching artifact peak around zero.

Fig. 2*b* shows a plot of mean FRET efficiencies as a function of distance for the seven DNA constructs. A clear monotonic decrease in transfer efficiency with distance is observed. The precision of the data decreases as the inter-dye separation increases above 19 bp (around 60 Å) because of overlap with the zero FRET peak. The solid line in Fig. 2*b* corresponds to the Förster prediction $E = 1/(1 + (R/R_0)^6$ for $R_0 = 65$ Å and is a visual guide for the data. The discrepancy between this value and $R_0 = 53$ Å, estimated from spectroscopic data, may be partly caused by the relatively large anisotropy (and hence $\kappa^2 \neq 2/3$, see below) measured for the two tethered dyes, uncertainty in the value of the factor $\gamma$ as discussed above, and fast distance fluctuations between the dyes. The precision for determining the distribution peak (mean FRET efficiency) is about $\pm 0.1$ $E$ for efficiencies ranging from $E = 0.5$ ($R = 60$ Å) to $E = 1$ ($R = 0$–30 Å). In terms of distance, this error bar translates into a precision of roughly $\pm 5$ Å in the 30- to 60-Å distance range.

**Subpopulations.** A key aspect of the ratiometric spFRET burst methodology, in contrast to simple ensemble measurements, is that it allows one to directly observe distributions and subpopulations. To demonstrate this capability, spFRET measurements were carried out on a mixture of DNA 7 and DNA 14 in approximately equimolar amounts. As can be seen in Fig. 3, in addition to the artifact peak around zero, two FRET peaks corresponding to DNA 7 ($E = 0.95$) and DNA 14 ($E = 0.75$) are clearly resolved. Furthermore, the area ratio of the fitted gaussians is 1.3:1, in good agreement with the composition of the mixture. The resolution that can be achieved is directly related to the mean FRET efficiency $E$ and the widths of the distributions. By using a Rayleigh type criterion, we estimate that two subpopulations separated by 0.2–0.3 $E$ units (corresponding to roughly $\pm 10$ Å in the 0.4- to 0.9-$E$ range) can be distinguished by using this approach.

**Widths of the Distributions.** For each of the DNA constructs in Fig. 2*b*, one can extract not only the mean but also the distribution width (SD) of the FRET peak. Fig. 2*c* shows the experimentally measured SDs versus mean FRET efficiencies. Among the various effects that contribute to the peak broadening, the dominant one is shot noise, which is a characteristic of single-molecule measurements with their inherently low signal counts. The emissions of both fluoropohores ($I_a$ and $I_d$) exhibit Poisson distributions, with mean values that depend on the excitation intensity and the photophysical characteristics of the dyes. For these low signals, the relative fluctuations, equal to the inverse of the square root of the mean value, play a significant role. This results in fluctuations in the ratio $E = I_a/(I_a + I_d)$, which put an intrinsic limit on the separation resolution that can be achieved by using this approach. To evaluate this limit, a simple model was used in which both emission channels $I_a$ and $I_d$ are described by Poisson variables. Their mean values are $E_m S$ and $(1 - E_m)S$, respectively, where $E_m$ is the mean transfer efficiency and $S$ is the sum of the signals in both channels. In practice, the shot noise is calculated for $S$ taken equal to the threshold $T$. Because only signals above this threshold are processed, they have a smaller relative shot noise, and this places an upper bound on the calculated values. The solid line in Fig. 2*c* displays this upper bound estimate for $T = 20$. The shot noise-induced fluctuations strongly depend on the FRET mean value with a maximum at $E = 0.5$. This simple model does not account for the diffusion of the molecules in the laser spot and the resulting variation in the excitation intensity. However, we have observed that this simple approach gives a reasonable estimate and that more complicated calculations lead only to changes of less than 10%, as will be discussed elsewhere. The experimentally determined widths for the

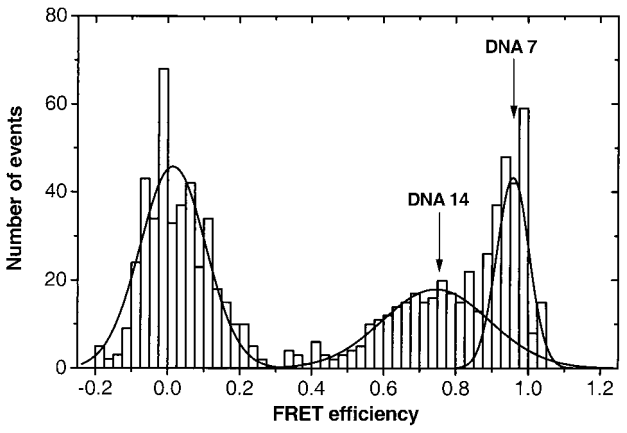


FIG. 3. FRET histogram of a 1:1 mixture of DNA 7 and 14 showing the separate subpopulations.

††Gaussian functions fit the histograms reasonably well when the mean FRET efficiency is not close to 1 or 0. For high efficiency ($E$ greater than 0.9), the FRET peak becomes asymmetric (Fig. 3). The gaussian fit then is not optimal though it does not lead to major discrepancies. A more detailed analysis of the fitting procedure will be presented elsewhere.

longer distances are significantly greater than the calculated values.

Besides shot noise, fluctuations in $E$ depend on fluctuations in the Förster radius $R_0$ and, more interestingly, on fluctuations in the distance between the two dyes. The dominant factor in $R_0$ fluctuations is $\kappa^2$, the orientational factor, which depends on the relative orientation of the two dipoles. A common assumption is that the two dyes are freely rotating on a time scale comparable to or faster than the fluorescence lifetime and that $\kappa^2$ can be dynamically averaged to a fixed value of $\kappa^2 = 2/3$ (22). To test whether this assumption holds for the present work, ensemble polarization anisotropy measurements were performed on the DNA constructs. It was found that both TMR and Cy5 attached to double-stranded DNA have large anisotropy values (around $r = 0.20$), indicating considerably hindered rotational diffusion. Therefore, $\kappa^2 \neq 2/3$ (affecting the mean FRET efficiency), and there could potentially be large $\kappa^2$ fluctuations, which could contribute to the FRET distribution widths.

Another source of broadening is fluctuations or distributions of distances between the two dyes. Distance distributions are of particular interest in conformational fluctuations in proteins, in end-to-end fluctuations of polymers, and in protein folding. Haas and coworkers (30) first developed ensemble time-resolved FRET techniques, data analysis, and modeling to extract such distributions from ensemble data. Single-molecule methods might shed new light on such measurements. It is noted that distance fluctuations in the DNA helix (transient bending, twisting, or local melting) and fluctuations in the long dye tethers are expected to be much faster than the 0.2-ms time resolution of the measurement. Such fast fluctuations are averaged out and should not contribute to the observed widths, though they might shift the mean value (31). It is possible, however, that slower distance fluctuations (at least on the millisecond time scale) caused by specific DNA-dye interactions are present. It was found that a longer integration time reduces the distribution widths. Therefore, depending on the application, time resolution can be traded for resolution of subpopulations. In the restriction enzyme study described below, a 1-ms integration time was used to enhance subpopulation resolution.

In summary, we speculate that the observed excess widths are partly a result of DNA-dye interactions, though we cannot rule out several other contributions mentioned above. These issues will be investigated in detail by using improved spacer constructs. In the future, diffusion combined with flow systems, faster hardware, and more sophisticated data analysis should help to better model, understand, and perhaps, reduce the broadening of the FRET distribution peak.

**Restriction Enzyme Cleavage.** The ability to examine individual subpopulations in a mixture can be used to study processes such as protein folding and enzymatic reactions, where the role of multiple pathways and reaction intermediates often is implicated. Using single-molecule FRET methods, one should be able to directly follow the evolution of individual conformational intermediates (provided that their lifetimes and the FRET efficiency peaks are resolved by the technique). It also has implications for the study of end-to-end distance distributions and subpopulations in polymers. To demonstrate this ability, a mixture of two distinct DNA subpopulations was subjected to enzymatic cleavage under conditions where only one subpopulation is cleaved.

The FRET histogram in Fig. 4*a* shows clearly resolved subpopulations in a mixture of DNA 7 and DNA 17. DNA 17 contains the *Eco*RI restriction enzyme sequence between the dye attachment points, whereas DNA7 does not. Upon cleavage, the donor and acceptor are separated for DNA 17 and FRET signals originating from this subpopulation should disappear. Fig. 4*b* shows a histogram of the same mixture after digestion by the restriction enzyme. The FRET peak corresponding to DNA 17 virtually disappears and there is a simultaneous increase in the "zero peak" corresponding to formation of product TMR-only DNA (DNA 7 serves as a reference because the starting mixture for Fig. 4 *a* and *b* is the same). In a steady-state ensemble experiment, one would merely observe a shift in the average FRET value, whereas, with ratiometric spFRET, it is possible to observe kinetic changes in each of the subpopulations.

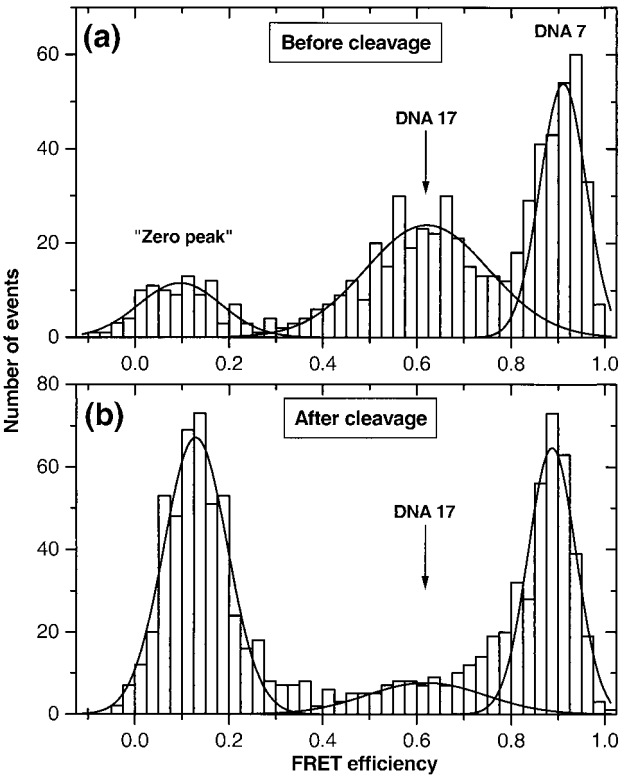


FIG. 4. Restriction endonuclease cleavage of DNA. Histograms of a mixture of DNA 7 (no *Eco*RI site) and DNA 17 (with *Eco*RI site) before (*a*) and after (*b*) the cleavage reaction. The FRET peak corresponding to DNA 17 virtually disappears after the cleavage reaction, and there is a simultaneous increase in the "zero peak."

**Denaturation of a DNA Hairpin.** A DNA hairpin consists of a double-stranded stem, the ends of which are connected by a single-stranded DNA loop. DNA hairpins can be reversibly denatured and can serve as simple, robust systems for folding studies and for developing methodology for the study of more complex biological systems. The hairpin used here was studied extensively at the ensemble level by Haasnoot and coworkers (17). They found that the hairpin is the only stable structure formed at room temperature, and it has a melting temperature of 47°C. Fig. 5 *Inset* shows a scheme of the donor-acceptor labeled hairpin.

Fig. 5 shows a denaturation curve of the DNA hairpin, measured by diffusion spFRET, for a series of urea concentrations between 0 and 8 M. All FRET histograms showed only one nonzero peak whose position changed as a function of urea concentration. Fig. 5 shows the mean (peak position) and distribution width versus urea concentration. A clear decrease in FRET efficiency is observed as the urea concentration increases, consistent with an increase in the population of unfolded hairpins. The increase in the widths with urea concentration could be caused by several factors discussed above. To check whether the urea-dependent changes in the transfer efficiency are indeed resulting from hairpin conformational changes, ensemble control experiments were performed. Relative quantum yields, spectral position, and polarization anisotropy were measured for both dyes (individu-

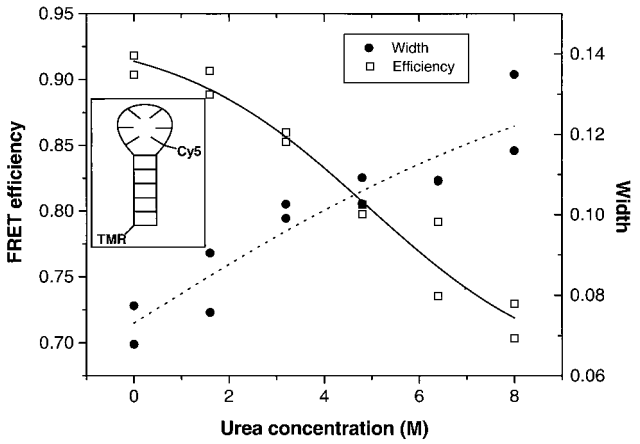


FIG. 5. DNA hairpin denaturation. The mean FRET efficiency and the widths as a function of urea concentration. (*Inset*) The donor-acceptor labeled haipin construct. The lines are visual guides for the data.

ally conjugated to the hairpin) as function of urea concentration. These varied very little (less than 20%) between 0 M and 8 M urea, contributing to small changes in $R_0$. Such small changes cannot explain the observed 0.2 change in $E$. We therefore conclude that the mean-efficiency curve in Fig. 5 reflects the denaturation of the hairpin.

It is interesting to note that only a gradual shift in the average position of the (single) high FRET peak is observed. No evidence for inter-conversion of two subpopulations, corresponding to folded and unfolded hairpins, was found. This result allows us to put a lower bound of about $5 \times 10^3\ s^{-1}$ (0.2 ms, the experimental time resolution) on the interconversion rate constants of the two forms. The rate constants for the closing and opening of the hairpin previously have been measured and are $2 \times 10^5\ s^{-1}$ and $5 \times 10^2\ s^{-1}$ in the absence of urea (17). In the presence of urea, the barrier, and consequently the lifetime of hairpin opening, will be reduced, consistent with our results.

## CONCLUSIONS

This work demonstrates that spFRET by ratiometric coincident burst detection is a viable technique for the study of freely diffusing biomolecules in solution. The $1/R^6$ Förster distance dependence was displayed, and it was shown that the diffusion methodology can be used to observe conformational subpopulations and distributions of biomolecules in solution without complications from surface interactions. The potential of the technique was illustrated by monitoring two reactions under equilibrium conditions, restriction enzyme cleavage of DNA, and the unfolding of a DNA hairpin. It should be possible to extend the methodology to the study of reactions under nonequilibrium conditions. In contrast to ensemble kinetics measurements, ratiometric burst techniques can monitor not only the time behavior of the relevant molecular observable ensemble average but also the kinetics of each of the subpopulations. Moreover, reaction intermediates that are very difficult to detect in ensembles because of inhomogeneity and lack of synchronization could, in principle, be identified in single-molecule experiments. Toward this end, the development of better fluorescence probes with improved photophysical and photobleaching characteristics and better data acquisition and analysis methods will greatly benefit and enhance such measurements.

Financial support for this work was provided by the National Institutes of Health (Grant No. GM49220), the Laboratory Directed Research and Development Program of Lawrence Berkeley National Laboratory under U.S. Department of Energy Contract No. DE-AC03-76SF00098, the Office of Naval Research Contract N0001498F0402, and the National Science Foundation under Grant No. CHE-971-4390. P.G.S. is a Howard Hughes Medical Institute Investigator.

1. Basché, T., Moerner, W. E., Orrit, M. & Wild, U. P., eds. (1997) *Single-Molecule Optical Detection, Imaging, and Spectroscopy* (Wiley, Cambridge).
2. Nie, S. M. & Zare, R. N. (1997) *Annu. Rev. Biophys. Biomol. Struct.* **26,** 567–596.
3. Xie, X. S. & Trautman, J. K. (1998) *Annu. Rev. Phys. Chem.* **49,** 441–480.
4. Lu, H. P., Xun, L. & Xie, X. S. (1998) *Science* **282,** 1877–1882.
5. Shera, E. B., Seitzinger, N. K., Davis, L. M., Keller, R. A. & Soper, S. A. (1990) *Chem. Phys. Lett.* **174,** 553–557.
6. Nie, S. M., Chiu, D. T. & Zare, R. N. (1994) *Science* **266,** 1018–1021.
7. Eigen, M. & Rigler, R. (1994) *Proc. Natl. Acad. Sci. USA* **91,** 5740–5747.
8. Sauer, M., Arden-Jacob, J., Drexhage, K. H., Göbel, F., Lieberwirth, U., Mühlegger, K., Müller, R., Wolfrum, J. & Zander, C. (1998) *BioImaging* **6,** 14–24.
9. Eggeling, C., Fries, J. R., Brand, L., Gunther, R. & Seidel, C. A. (1998) *Proc. Natl. Acad. Sci. USA* **95,** 1556–1561.
10. Edman, L., Mets, U. & Rigler, R. (1996) *Proc. Natl. Acad. Sci. USA* **93,** 6710–6715.
11. Maiti, S., Haupts, U. & Webb, W. W. (1997) *Proc. Natl. Acad. Sci. USA* **94,** 11753–11757.
12. Bonnet, G., Krichevsky, O. & Libchaber, A. (1998) *Proc. Natl. Acad. Sci. USA* **95,** 8602–8606.
13. Kettling, U., Koltermann, A., Schwille, P. & Eigen, M. (1998) *Proc. Natl. Acad. Sci. USA* **95,** 1416–1420.
14. Soper, S. A., Davis, L. M. & Shera, E. B. (1992) *J. Opt. Soc. Am. B* **9,** 1761–1769.
15. Schwille, P., Meyer-Almes, F. J. & Rigler, R. (1997) *Biophys. J.* **72,** 1878–1886.
16. Ha, T., Enderle, T., Ogletree, D. F., Chemla, D. S., Selvin, P. R. & Weiss, S. (1996) *Proc. Natl. Acad. Sci. USA* **93,** 6264–6268.
17. Haasnoot, C. A., de Bruin, S. H., Berendsen, R. G., Janssen, H. G., Binnendijk, T. J., Hilbers, C. W., van der Marel, G. A. & van Boom, J. H. (1983) *J. Biomol. Struct. Dyn.* **1,** 115–129.
18. Ha, T., Enderle, T., Chemla, D. S. & Weiss, S. (1996) *IEEE J. Quant. Electron.* **2,** 1115–1128.
19. Clegg, R. M., Murchie, A. I. H., Zechel, A. & Lilley, D. M. J. (1993) *Proc. Natl. Acad. Sci. USA* **90,** 2994–2998.
20. Jares-Erijman, E. A. & Jovin, T. M. (1996) *J. Mol. Biol.* **257,** 597–617.
21. Dickerson, R. E. (1992) *Methods Enzymol.* **211,** 67–111.
22. Cantor, C. R. & Schimmel, P. R. (1980) *Biophysical Chemistry* (Freeman, San Francisco).
23. Stryer, L. & Haugland, R. P. (1967) *Proc. Natl. Acad. Sci. USA* **58,** 719–730.
24. Schütz, G. J., Trabesinger, W. & Schmidt, T. (1998) *Biophys. J.* **74,** 2223–2226.
25. Ha, T., Ting, A. Y., Liang, J., Caldwell, B., Deniz, A. A., Schultz, P. G., Chemla, D. S. & Weiss, S. (1999) *Proc. Natl. Acad. Sci. USA* **96,** 893–898.
26. Dovichi, N. J. (1997) in *Single-Molecule Optical Detection, Imaging, and Spectroscopy,* eds. Basché, T., Moerner, W. E., Orrit, M. & Wild, U. P. (Wiley, Cambridge), pp. 223–243.
27. Hagerman, P. J. (1988) *Annu. Rev. Biophys. Biophys. Chem.* **17,** 265–286.
28. Peck, K., Stryer, L., Glazer, A. N. & Mathies, R. A. (1989) *Proc. Natl. Acad. Sci. USA* **86,** 4087–4091.
29. Funatsu, T., Harada, Y., Tokunaga, M., Saito, K. & Yanagida, T. (1995) *Nature (London)* **374,** 555–559.
30. Haas, E., Wilchek, M., Katchalski-Katzir, E. & Steinberg, I. Z. (1975) *Proc. Natl. Acad. Sci. USA* **72,** 1807–1811.
31. Cantor, C. R. & Pechukas, P. (1971) *Proc. Natl. Acad. Sci. USA* **68,** 2099–2101.